


Article

High-Ratio Nonlinear Compression of Picosecond Lasers Based on Thin Plates

Kainan Zhou ^{1,2}, Zhaoli Li ^{2,*}, Yanlei Zuo ², Zhaohui Wu ², Xiaoming Zeng ², Xiao Wang ², Xiaodong Wang ², Jie Mu ² and Guoying Feng ¹ 

¹ Institute of Laser and Micro/Nano Engineering, College of Electronics and Information Engineering, Sichuan University, Chengdu 610065, China; zhoukainan@caep.cn (K.Z.); guoying_feng@scu.edu.cn (G.F.)

² Laser Fusion Research Center, China Academy of Engineering Physics, Mianyang 621900, China; zuoyanlei@tsinghua.org.cn (Y.Z.); wuzhaohui20050@163.com (Z.W.); 13398364617@163.com (X.Z.); wangxiaocn@263.net (X.W.); 13990186517@139.com (X.W.); mujiebest@163.com (J.M.)

* Correspondence: lizhaoli@caep.cn

Abstract: Nonlinear compression, as a newly developed post-processing technique, holds the potential to overcome the limitations of gain media and significantly reduce the pulse width of emitted laser pulses. While most existing research has focused on the compression of femtosecond pulses, the methods employed differ substantially from those used for picosecond laser nonlinear compression. In this study, we experimentally investigated the high-ratio nonlinear compression of a picosecond laser using a thin-plate-based approach. A 1 ps, 0.55 mJ laser pulse was successfully compressed to 69.6 fs with an energy of 0.26 mJ through a two-stage nonlinear compression process. Beam spatial quality was well preserved by employing apertures to eliminate conical emissions. These results pave the way for advancements in high-peak-power, high-repetition-rate laser systems, offering a promising route for future applications.

Keywords: nonlinear compression; self-phase modulation; dispersion; picosecond laser



Received: 2 December 2024

Revised: 24 December 2024

Accepted: 26 December 2024

Published: 30 December 2024

Citation: Zhou, K.; Li, Z.; Zuo, Y.; Wu, Z.; Zeng, X.; Wang, X.; Wang, X.; Mu, J.; Feng, G. High-Ratio Nonlinear Compression of Picosecond Lasers Based on Thin Plates. *Photonics* **2025**, *12*, 21. <https://doi.org/10.3390/photonics12010021>

Copyright: © 2024 by the authors. Licensee MDPI, Basel, Switzerland. This article is an open access article distributed under the terms and conditions of the Creative Commons Attribution (CC BY) license (<https://creativecommons.org/licenses/by/4.0/>).

1. Introduction

High-power, high-repetition-rate lasers have promising applications in cutting-edge science and technology, including high-energy particle beam generation and novel X/γ-ray sources [1,2], laser-based precision micromachining [3,4], ultrafast spectroscopy [5–7], infrared and terahertz radiation sources [8,9], air pollution monitoring [10], advanced sensor technologies [11,12], weather control [13–15], space communication [16,17], among others. Yb³⁺-doped solid-state lasers have emerged as a leading platform for developing high-power, high-repetition-rate lasers due to their high quantum efficiency and excellent thermal conductivity. To date, the average output power of Yb³⁺-doped Innoslab [18], thin-disk [19], and fiber [20] lasers has reached the kilowatt level. However, the relatively narrow gain bandwidth of Yb³⁺ ions constrains the achievable pulse duration to the picosecond regime. Compressing the pulse duration to the femtosecond scale would significantly enhance the peak power, thereby broadening their application potential across a range of advanced scientific and technological fields.

The pulse duration of a laser is fundamentally constrained by the time–frequency relationship described by Fourier transform principles, which dictate that a minimum pulse width requires a correspondingly broad spectral bandwidth. To achieve the shortest possible pulses, nonlinear compression techniques have been developed. These techniques exploit the interaction between laser pulses and nonlinear media, leveraging the self-phase

modulation (SPM) effect to broaden the pulse spectrum. Subsequently, dispersion compensation is applied to counteract the temporal broadening introduced during spectral expansion, enabling the compression of pulse duration. Initially, optical fibers were commonly used as the medium for producing the SPM effect. However, the self-focusing threshold and material damage limits of optical fibers rendered them unsuitable for high-power, high-energy ultrashort pulse compression. To enable spectral broadening at higher energy levels, researchers have explored the use of thin plates as the broadening medium. In 2013, Aleksandr A. Voronin et al. [21] proposed the use of fused silica thin plates to broaden laser spectrums, with simulation results demonstrating that cycle-level broadband laser pulses can be achieved. Subsequently, in 2016, Philippe Lassonde et al. [22] focused a 30 mJ, 40 fs laser pulse onto a 3 mm thick fused silica or TF12 glass plate. The broadened laser pulse was then compressed to 25.5 mJ, 16 fs using chirp mirrors with a total dispersion of -220 fs^2 . The energy transmission rate was 85%. Since then, other groups have reported nonlinear compression results by directly focusing on thin plates.

Another efficient nonlinear compression method is based on the multi-pass cell (MPC) technique. When a laser pulse traverses the MPC multiple times, with thin plates or inert gas serving as Kerr media, the laser pulse gradually accumulates the B-integral through repeated nonlinear interactions with the Kerr medium. In 2006, Jan Schulte et al. [23] applied the MPC technique for nonlinear compression. They inserted a fused silica plate at the center of the MPC. After 18 reflections, a 53 μJ , 850 fs laser pulse was spectrally broadened from 1.6 nm to >13.5 nm bandwidth and then compressed to 45 μJ , 170 fs using two chirped mirrors. In 2018, Moritz Ueffing et al. [24] injected neon, argon, or nitrogen gas into the MPC as a Kerr medium, compressing the 2 mJ, 210 fs laser pulse to 1.86 mJ, 37 fs. In the same year, L. Lavenu et al. [25] demonstrated nonlinear compression of a Yb-doped fiber laser source in an MPC filled with 7 atm argon gas. The 160 μJ , 275 fs input pulses were compressed down to 135 μJ , 33 fs at the output. Other groups have also demonstrated nonlinear compression results based on the MPC technique.

Most of the above experiments were aimed at compressing femtosecond pulses, and the overall schemes differed significantly from those used for picosecond laser compression. While some groups [26–30] reported results on picosecond laser compression, these studies were all based on the MPC technique or hollow-core fiber [31,32]. For high-energy picosecond lasers, the MPC technique needs a large space to place the MPC (for mJ-level laser pulses, the length of the MPC would be several meters). Fabrication, installation, and transportation of the MPC would be very inconvenient and uneconomical. Using hollow-core fiber may encounter more serious problems, such as thermal load, self-focusing, filamentation, and high-order mode conversion. Compressing picosecond lasers by directly focusing onto thin plates offers a compact and portable alternative, which has not been reported—to the best of our knowledge. Although there have been some numerical simulation works [33,34] discussing the possibility of thin-plate-based picosecond laser compression, all the experimental works have so far been carried out using femtosecond lasers. The widest laser pulse compressed by thin-plate-based nonlinear compression, as far as we know, was 350 fs [35] and was compressed to 124 fs. In this article, we report our experimental results on the nonlinear compression of a picosecond laser by directly focusing it onto thin plates. A 0.55 mJ, 1 ps laser was compressed to 0.26 mJ, 69.6 fs through a two-stage nonlinear compression process, with its spectral width broadened from 4 nm to 36 nm. The experimental results fit well with numerical simulation works [33,34] and our numerical simulation program. Section 3 shows our optical path design and simulation results. Section 3 also shows the experimental setup and compression results. Section 4 discusses the spatial beam quality of the compressed pulse. Finally, Section 5 gives the conclusions of the study.

2. Two-Stage Thin-Plate-Based Nonlinear Compression: Design

To explore the feasibility of high-ratio picosecond laser compression using the thin-plate-based nonlinear compression technique, we adopt a far-field focusing method based on the existing picosecond laser with parameters of 1030 nm/1 mJ/1 kHz/1 ps/ \varnothing 2 mm in our laboratory, focusing the picosecond laser onto a fused silica thin plate. Through the Kerr effect in the thin plate, we can achieve a certain amount of spectral broadening. Additionally, the Kerr lens' effect on the plate allows the laser to be refocused on the next plate. By using multiple plates, we can obtain a sufficiently broadened spectrum. Subsequently, compression is performed using a chirped mirror. Multiple plates are added until the laser spectrum no longer shows significant broadening, thus completing the design of the spectral broadening part of the nonlinear compression. We use our in-house numerical simulation program to simulate the nonlinear compression process and calculate the group delay dispersion (GDD) that needs to be compensated for. The pulse energy is limited to 0.5 mJ. The laser pulse is focused through a lens with a focal length of 300 mm, with the laser radius at the focal point being 0.188 mm. At this point, the energy flow density of the laser at the focal point is 0.9 J/cm², which is far below the damage threshold of fused silica (about 3 J/cm²@1 ps). The first plate, with a thickness of 1 mm, is placed at the focal point. After passing through the first plate, the laser is refocused, as shown in Figure 1. After transmission through the air for 25 mm, the laser refocuses on the second focal point, with the laser intensity rising to a maximum of 1.62 TW/cm² and an energy flow density of 1.72 J/cm², which is still below the damage threshold of fused silica. The second plate is then placed in this position. Similarly, the distances between the third and fourth plates and the previous plate are 35 mm and 30 mm, respectively. The spectral and temporal profile of the laser pulse before and after spreading through the first stage of nonlinear compression are shown in Figure 2. The results show that the bottom width of the laser bandwidth expanded from 3.2 nm (10% width) to 11.6 nm, accompanied by a group delay dispersion of 61,328 fs². After compensating for the group delay dispersion, the pulse width (full width at half maximum) of the laser was compressed from 1000 fs to 297 fs. Note that due to estimating the thickness of the focusing lens at about 1 cm, the lens also had a small contribution to the B-integral (~0.43), which was not included in the simulation.

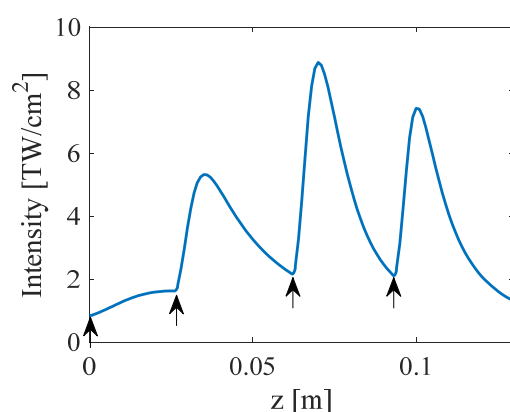


Figure 1. Changes in maximum laser intensity with position in the first stage of nonlinear compression. The black arrows indicate the positions of the thin plates.

After the first stage of compression, we add another stage of thin-plate compression to achieve cascaded high-ratio nonlinear compression. The energy transmittance rate of the laser pulse after the first stage of nonlinear compression is conservatively estimated to be 60%, with a pulse width of 300 fs; the diameter of the laser remains at 2 mm after collimation. When this laser pulse is focused through a lens with a focal length of 250 mm,

the laser diameter at the focal point is 0.157 mm. The energy flux density of the laser pulse at the focal point is 0.77 J/cm^2 , which is less than the damage threshold of fused silica (about $2 \text{ J/cm}^2@300 \text{ fs}$), and the intensity is increased to 2.4 TW/cm^2 . Due to the higher intensity of the laser pulse at this stage of compression, it is expected that the laser pulse will achieve a greater compression ratio. The first thin plate, with a thickness of 1 mm, is placed at the focal point. After passing through this thin plate, the laser pulse propagates freely in the air, and the laser intensity first increases and then decreases, as shown in Figure 3. The light intensity decreases to 2.4 TW/cm^2 at the 60 mm position; thus, the second thin plate is placed at this position. Similarly, the distances between the third and fourth thin plates and the previous plate are 40 mm and 40 mm, respectively. According to the figure, the distance required to decrease the laser intensity to its original value is too small, hence we do not insert the fifth plate. The spectrum and temporal profile of the laser pulse before and after spreading through the second stage of nonlinear compression are shown in Figure 4. The bottom width of the laser bandwidth expands from 11.76 nm to 63.86 nm, resulting in a group delay dispersion of 3004 fs^2 . After compensating for all group delay dispersions, the pulse width (full width at half maximum) of the laser is compressed from 300 fs to 49 fs. This way, through the second-stage compression, the laser pulse width is compressed by about 6 times, thus achieving a total compression ratio of 20 times.

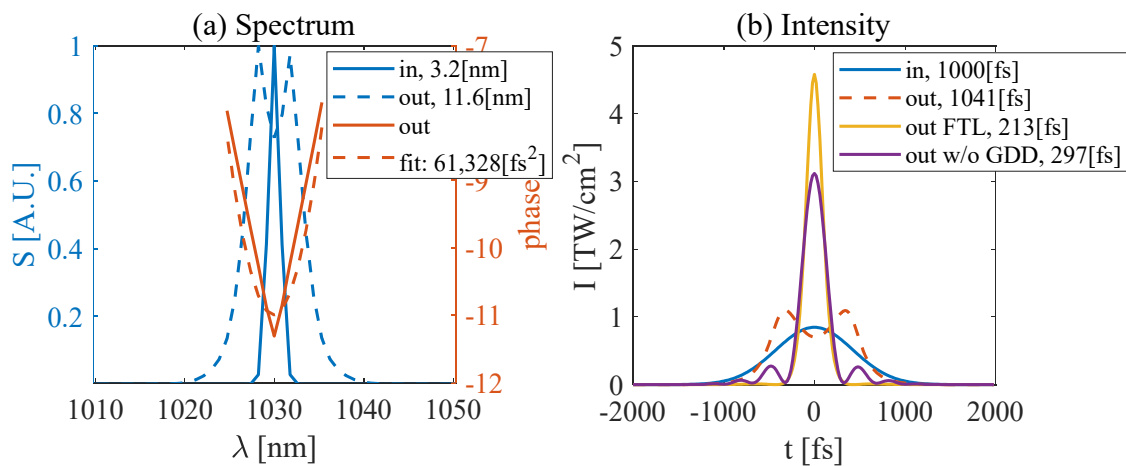


Figure 2. (a) Spectrum and (b) temporal profile of the laser pulse before and after spreading through the first stage of nonlinear compression.

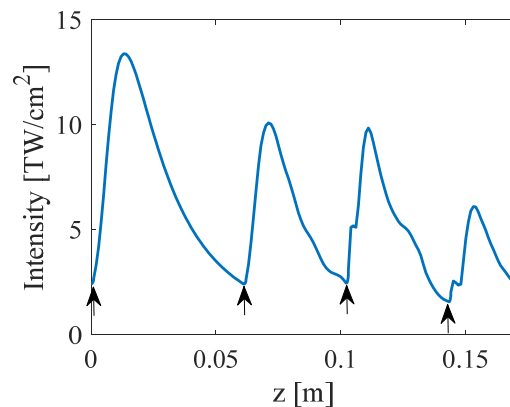


Figure 3. Changes in maximum laser intensity with position in the second stage of nonlinear compression. The black arrows indicate the positions of the thin plates.

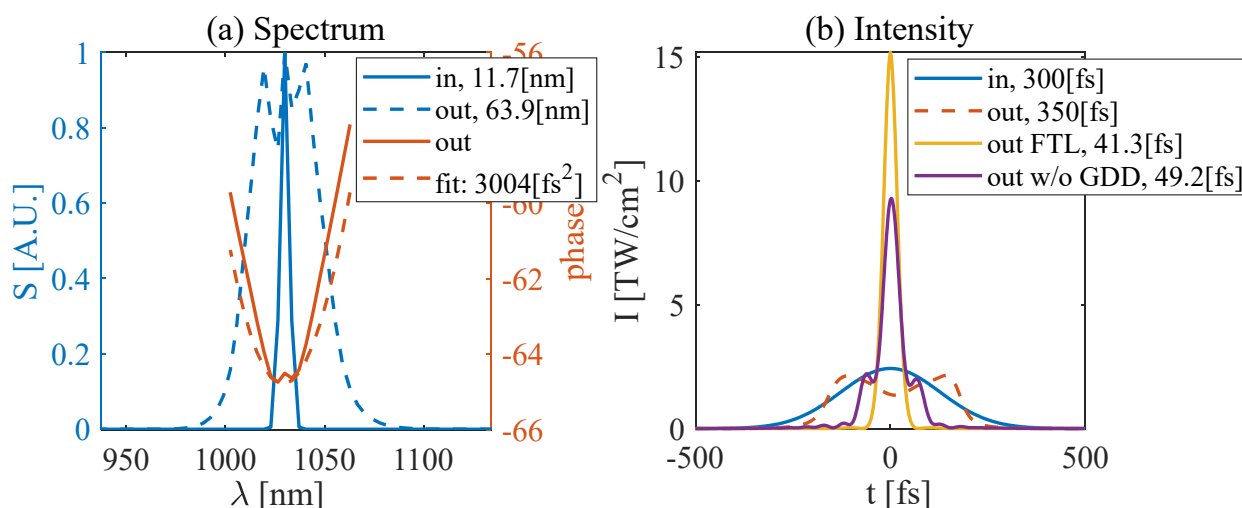


Figure 4. (a) Spectrum and (b) temporal profile of the laser pulse before and after spreading through the second stage of nonlinear compression.

3. Two-Stage Thin-Plate-Based Nonlinear Compression: Experiment

The laser system used in this work consists of a Yb-doped mode-locked fiber oscillator and a Yb:YAG regenerative amplifier, delivering 1 mJ, 1 ps, 1 kHz laser pulses with a central wavelength of 1030 nm. In the experiment, we set the maximum laser energy to 0.55 mJ. The experimental setup is shown in Figure 5. The laser pulse was first focused by a convex lens with a 300 mm focal length. Four 1 mm thick fused silica thin plates were used as Kerr medium and placed at focal points at 30 mm, 25 mm, and 25 mm distances. The laser pulse was then collimated by another convex lens with a 300 mm focal length after its spectrum was broadened. The spectrum-broadened laser was compressed using six chirped mirrors, which provided a total group delay dispersion of $-48,000$ fs² through 24 reflections to compensate for the dispersion introduced by the thin plates. The compressed pulse then passed through the second stage of nonlinear compression, which had basically the same configuration as the first stage. The laser pulse was first focused by a convex lens with a 250 mm focal length. Four 1 mm thick fused silica thin plates were placed at focal points at 25 mm, 33 mm, and 27 mm distances. The laser pulse was then collimated by another convex lens with a 300 mm focal length, and then two chirped mirrors were used to provide a total group delay dispersion of -3000 fs² through six reflections. Two apertures were placed at the end of each nonlinear compression module to cut off the conical emission. The sizes of the apertures were finely adjusted to 3.5 mm and 4.5 mm to precisely cut off the conical emission.

To reduce the laser reflections, all thin plates were coated with AR coatings to prevent them from rotating to Brewster's angle. The incident angles were rotated slightly from 0° to avoid a backward-reflected laser. The spectra of the output pulses after the first and second stages of nonlinear compression are shown in Figure 6. At low energy, the spectral width of the input pulse was approximately 1029.1–1032.9 nm. When the laser energy was increased to 0.55 mJ, the laser spectrum was broadened to 1024.5–1037.8 nm in the first stage, and further to 1013–1047 nm in the second stage. When the laser energy increased from 0.37 mJ to 0.55 mJ, the spectral width significantly expanded in the first stage; however, in the second stage, the spectral shape changed significantly while the spectral width increased only slightly.

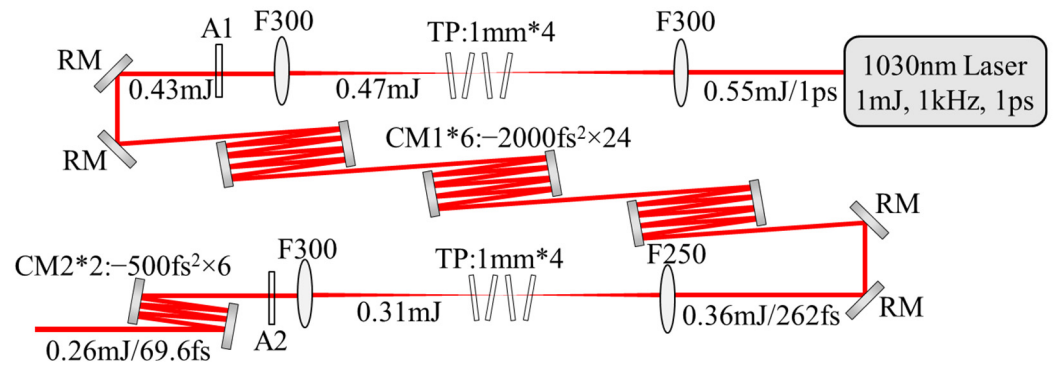


Figure 5. Schematic diagram of the nonlinear compression experimental setup. F: focusing lens, TP: fused silica plates, A: aperture, RM: reflecting mirrors, CM: chirped mirrors.

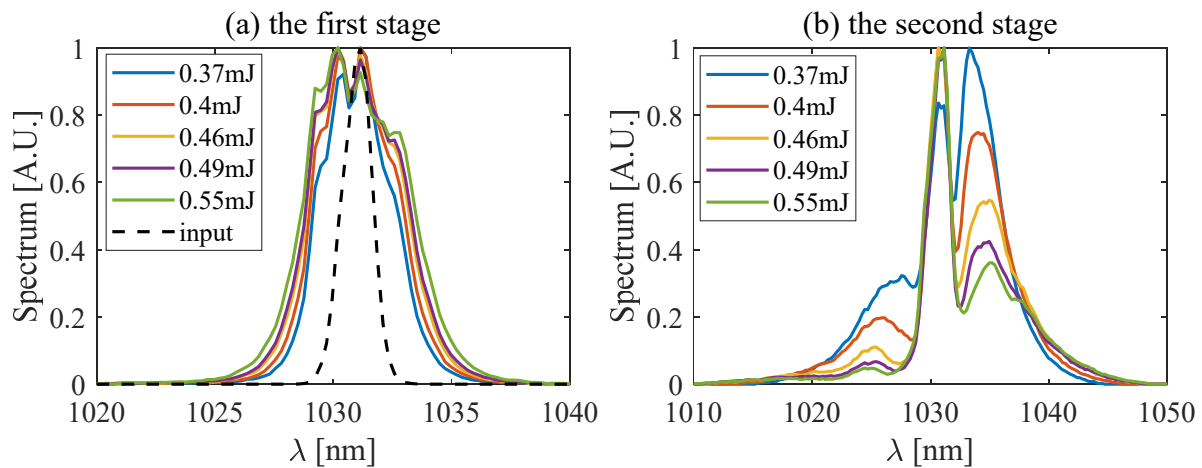


Figure 6. Spectrum of the output laser pulse after (a) the first stage and (b) the second stage of nonlinear compression.

The FROG signals of the output pulse with 0.55 mJ laser energy are shown in Figure 7. When the input laser energy was set to 0.55 mJ, the pulse duration was compressed to 69.6 fs after two-stage nonlinear compression. The spectral phase curve was flat around the central wavelength, indicating that the dispersion of the laser pulse was precisely compensated for by the chirped mirrors. The duration of the output pulses after the first and the second stages of nonlinear compression are shown in Figure 8. It can be observed that in the first stage, the pulse duration decreased with increasing laser energy; however, in the second stage, the pulse duration remained unchanged with increasing laser energy. This is consistent with the spectrum measurement results.

When the incident laser energy was set to 0.55 mJ, the output laser energy decreased to 0.47 mJ after passing through the first four thin plates and to 0.43 mJ after passing through the first aperture. Although the reflection mirrors and the chirped mirrors have high reflection ratios, after multiple reflections and edge transmissions, the laser energy still decreased to 0.36 mJ when entering the second stage of nonlinear compression. The energy of the laser pulse decreased to 0.26 mJ upon being emitted from the second stage of nonlinear compression, resulting in a total transmission ratio of 47%.

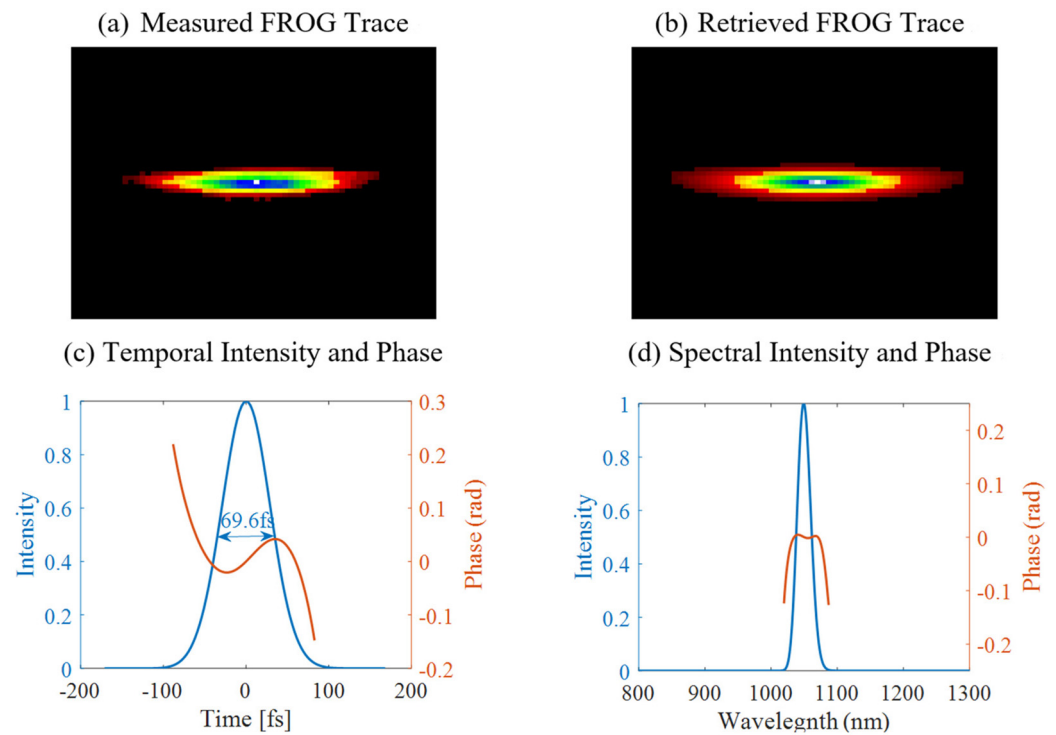


Figure 7. The FROG signals of the output pulse when the laser energy is 0.55 mJ. (a) Measured FROG trace; (b) retrieved FROG trace; (c) temporal intensity and phase; (d) spectral intensity and phase.

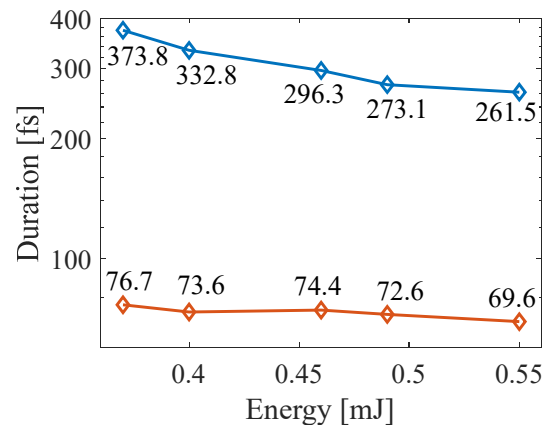


Figure 8. Pulse widths of the compressed pulse after one (blue) and two (red) stages of nonlinear compression with different laser energies and different group delay dispersion compensation amounts.

4. Spatial Profile of the Laser Pulse

The near field and far field of the input pulse are shown in Figure 9. The far field was obtained by focusing the laser pulse using a convex lens with a 500 mm focal length. The near field of the input pulse was close to the ideal Gaussian distribution with small ovality. The diameter of the near field was 2 mm. After compression, the diameter of the far-field was 0.3 mm, close to the calculated value of 0.31 mm. The profile of the far field was very close to a perfect circle, indicating that the spatial beam quality is ideal. The near field and the far field of the output pulse after the nonlinear compression are shown in Figure 10. In the near field shown in Figure 10a, the main lobe is still close to the Gaussian distribution, but some conical emission circles exist outside the main lobe. The diameter of the main lobe was 3 mm, and the diameters of the first and second rings of conical emission were 5.5 mm and 8 mm, respectively. The far field of the output pulse after filtering out the conical emission is shown in Figure 10b. The diameter of the far field was 0.27 mm, larger

than the calculated value of 0.21 mm. To avoid damaging the chirped mirrors, the output pulse of the second nonlinear compression stage was designed to have a smaller defocusing than collimated; hence, the real focal position was 600 mm away from the focusing lens. If the focal length is taken to be 600 mm, the calculated diameter of the focal spot will be 0.25 mm, close to the measured value. There was a bleed halo around the spot, and the spot itself had a little distortion, suggesting that the spatial beam quality may have undergone a minor degradation. By comparing the maximum value of the image data and the exposure times, and including the beam diameters at the focal points and the focal lengths, we find that the peak influence in the far field increased 6.39 times after the nonlinear compression, which is slightly lower than the maximum value of 6.79.

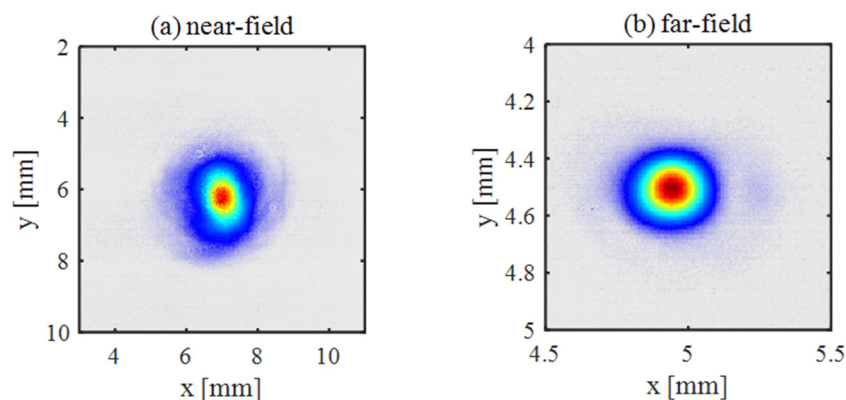


Figure 9. (a) The near field and (b) the far field of the incident pulse.

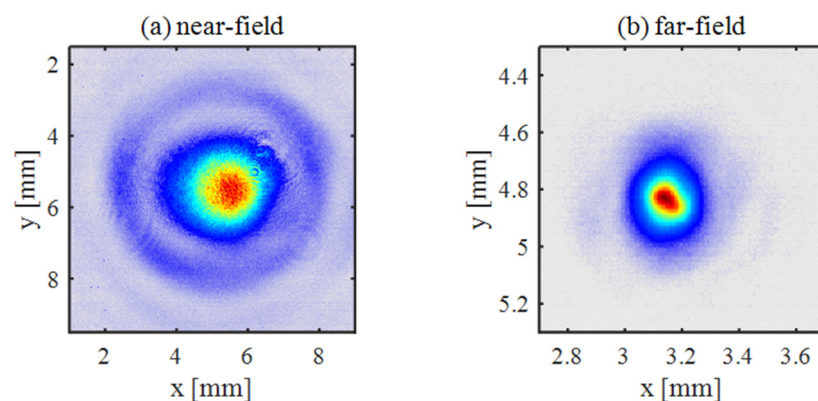


Figure 10. (a) The near field and (b) the far field of the output pulse.

5. Discussion

The newly emerging nonlinear compression technique has the potential to significantly reduce the pulse widths of lasers, thereby greatly enhancing their peak power. However, achieving high-ratio compression of picosecond lasers remains a significant challenge. Existing reports on nonlinear compression of picosecond lasers are all based on multi-pass cells or hollow-core fibers. Nonlinear compression based on multi-pass cells can achieve a high compression ratio and a high energy transmission rate and has been demonstrated to compress a 112 mJ, 1.3 ps laser pulse to 37 fs using a 9 m long gas-filled multi-pass cell [28]. However, when applying a multi-pass cell to the compression of joule-level lasers, the length of the multi-pass cell needs to be at least tens of meters long, making it quite bulky. Moreover, high-energy picosecond lasers usually have a flat top spatial distribution, which makes the mode matching of multi-pass cells a problem. Nonlinear compression based on hollow-core fibers has achieved effective compression of tens of millijoules and hundreds of femtoseconds of laser pulses [34], but its energy transmission rate is low. This

leads to another problem, i.e., a huge thermal load on the hollow-core fiber during the compression of joule-level lasers. Additionally, it faces other issues, such as self-focusing, filamentation, and high-order mode conversion, when the laser energy is high. Therefore, both of these technologies are not suitable for compressing high-energy picosecond lasers. As a result, the cascade nonlinear compression technique based on solid thin plates appears to be a more promising approach for compressing high-energy picosecond lasers. For millijoule lasers, one can use a focus lens to achieve sufficiently high intensity at the focal point. When the laser energy increases, the focal length of the lens becomes very long, at which point the lens can be replaced by a cylindrical mirror, a microlens array, or a beam-expander/reducing lens group to obtain a more compact optical path structure. Our experimental results show that although the compression ratio in the first stage of thin-plate-based nonlinear compression of picosecond laser is relatively low, one can increase the laser intensity at the focal point in the subsequent stages, thereby achieving a higher compression ratio in the subsequent stages of nonlinear compression. The distances between the thin plates in the experiment deviated slightly from the design values because the incident pulse of the first and second stages of compression had some focusing and divergence, respectively; thus, we adjusted the distances to get the best compression effect. After two stages of compression, the beam quality of the laser in both near and far fields remains high because the continuous focusing process plays a spatial filtering role. The energy loss of the laser is relatively high after two stages of compression. This is due to the conical radiation generated by the thin plates and the continuous reflection and edge incidence of the chirped mirrors. By optimizing the GDD compensation amount and the optical path structure of the chirped mirrors, the energy loss caused by the second factor is expected to be completely eliminated, thereby achieving a higher energy transmission rate. We experimentally verified the feasibility of high-ratio compression of millijoule-level picosecond lasers through cascade nonlinear compression based on thin plates, and when the laser energy increases, only slight modifications of the scheme are needed to scale up the scheme for effective compression of joule-level picosecond lasers.

6. Conclusions

This study experimentally investigated the process of nonlinear compression of picosecond lasers using thin plates. The experimental results showed that a picosecond laser with 0.55 mJ and 1 ps pulse duration was compressed to 0.26 mJ and 69.6 fs through two-stage, directly focusing, nonlinear compression, which, as far as we know, was the first demonstration of the method for picosecond pulses in the one-pass scheme (contrary to the multi-pass cell). The dispersion of the output pulse was precisely compensated for by the chirped mirrors, as measured by the FROG. Several rings of conical emission appeared in the near field of the output pulse; these were filtered out by the apertures. Some distortion and halos were also observed in the far field of the output pulse, suggesting a slight degradation of spatial beam quality. The laser energy decreased to about half after the nonlinear compression, mainly due to the conical emission and multiple reflections and edge transmissions of the chirp mirrors. The research results provide valuable insights into the high-ratio nonlinear compression of high-energy picosecond lasers.

Author Contributions: Conceptualization, Z.L. and X.Z.; Methodology, Z.L. and Y.Z.; software, Z.L.; validation, Z.L.; formal analysis, Z.L.; investigation, K.Z. and Z.L.; resources, Z.W., X.Z., X.W. (Xiao Wang), X.W. (Xiaodong Wang), J.M. and G.F.; data curation, Z.L.; writing—original draft preparation, K.Z. and Z.L.; writing—review and editing, K.Z. and Z.L.; visualization, Z.L.; supervision, Z.L. and G.F.; project administration, Z.L.; funding acquisition, K.Z., Z.L. and Y.Z. All authors have read and agreed to the published version of the manuscript.

Funding: This research is funded by the National Key Laboratory of Plasma Physics (6142A04220204, JCKYS2023212802, JCKYS2024212806) and the National Key Research and Development Program of China (2022YFB3606305).

Institutional Review Board Statement: Not applicable.

Informed Consent Statement: Not applicable.

Data Availability Statement: The raw data supporting the conclusions of this article will be made available by the authors on request.

Conflicts of Interest: The authors declare no conflict of interest.

References

1. Joshi, C.; Corde, S.; Mori, W.B. Perspectives on the generation of electron beams from plasma-based accelerators and their near and long term applications. *Phys. Plasmas* **2020**, *27*, 070602. [[CrossRef](#)]
2. Ziegler, T.; Göthel, I.; Assenbaum, S.; Bernert, C.; Brack, F.-E.; Cowan, T.E.; Dover, N.P.; Gaus, L.; Kluge, T.; Kraft, S.; et al. Laser-driven high-energy proton beams from cascaded acceleration regimes. *Nat. Phys.* **2024**, *20*, 1211–1216. [[CrossRef](#)]
3. Götte, N.; Winkler, T.; Meinel, T.; Kusserow, T.; Zielinski, B.; Sarpe, C.; Senftleben, A.; Hillmer, H.; Baumert, T. Temporal airy pulses for controlled high aspect ratio nanomachining of dielectrics. *Optica* **2016**, *3*, 389. [[CrossRef](#)]
4. Butkus, S. Micromachining of transparent, semiconducting and metallic substrates using femtosecond laser beams. *J. Laser Micro/Nanoeng.* **2016**, *11*, 81. [[CrossRef](#)]
5. Hauri, C.; Kornelis, W.; Helbing, F.; Heinrich, A.; Couairon, A.; Mysyrowicz, A.; Biegert, J.; Keller, U. Generation of intense, carrier-envelope phase-locked few-cycle laser pulses through filamentation. *Appl. Phys. B* **2004**, *79*, 673. [[CrossRef](#)]
6. Hauri, C.P.; Guandalini, A.; Eckle, P.; Kornelis, W.; Biegert, J.; Keller, U. Generation of intense few-cycle laser pulses through filamentation parameter dependence. *Opt. Express* **2005**, *13*, 7541. [[CrossRef](#)]
7. Théberge, F.; Aközbek, N.; Liu, W.; Becker, A.; Chin, S.L. Tunable ultrashort laser pulses generated through filamentation in gases. *Phys. Rev. Lett.* **2006**, *97*, 023904. [[CrossRef](#)]
8. Zhou, X.; Lin, Y.; Chan, Y.; Deng, F.; Zhang, J. Coherent generation and control of tunable narrowband THz radiation from a laser-induced air-plasma filament. *Opt. Lett.* **2023**, *48*, 2881. [[CrossRef](#)]
9. Pac Chong, M.L.; Garriga Francis, K.J.; Yiwen, E.; Zhang, X.C. Single-shot local measurement of terahertz correlated second harmonic generation in laser air plasma filaments. *Opt. Lett.* **2024**, *49*, 226. [[CrossRef](#)]
10. Kasparian, J.; Rodriguez, M.; Méjean, G.; Yu, J.; Salmon, E.; Wille, H.; Bourayou, R.; Frey, S.; André, Y.-B.; Mysyrowicz, A.; et al. White-light filaments for atmospheric analysis. *Science* **2003**, *301*, 61.
11. Chin, S.L.; Xu, H.L.; Luo, Q.; Théberge, F.; Liu, W.; Daigle, J.F.; Kamali, Y.; Simard, P.T.; Bernhardt, J.; Hosseini, S.A.; et al. Filamentation “remote” sensing of chemical and biological agents/pollutants using only one femtosecond laser source. *Appl. Phys. B* **2009**, *95*, 1. [[CrossRef](#)]
12. Dicaire, I.; Jukna, V.; Praz, C.; Milián, C.; Summerer, L.; Couairon, A. Spaceborne laser filamentation for atmospheric remote sensing. *Laser Photonics Rev.* **2016**, *10*, 481. [[CrossRef](#)]
13. Liu, Y.; Sun, H.; Liu, J.; Liang, H.; Ju, J.; Wang, T.; Tian, Y.; Wang, C.; Liu, Y.; Chin, S.L.; et al. Laser-filamentation induced water condensation and snow formation in a cloud chamber filled with different ambient gases. *Opt. Express* **2016**, *24*, 7364. [[CrossRef](#)] [[PubMed](#)]
14. Houard, A.; Walch, P.; Produit, T.; Moreno, V.; Mahieu, B.; Sunjerga, A.; Herkommer, C.; Mostajabi, A.; Andral, U.; André, Y.-B.; et al. Laser-guided lightning. *Nat. Photonics* **2023**, *17*, 231. [[CrossRef](#)]
15. Wolf, J.P. Short-pulse lasers for weather control. *Rep. Prog. Phys.* **2018**, *81*, 026001. [[CrossRef](#)]
16. Jhajj, N.; Rosenthal, E.; Birnbaum, R.; Wahlstrand, J.; Milchberg, H. Demonstration of long-lived high-power optical waveguides in air. *Phys. Rev. X* **2014**, *4*, 011027.
17. Rosenthal, E.; Jhajj, N.; Wahlstrand, J.K.; Milchberg, H. Collection of remote optical signals by air waveguides. *Optica* **2014**, *1*, 5. [[CrossRef](#)]
18. Russbueldt, P.; Mans, T.; Weitenberg, J.; Hoffmann, H.D.; Poprawe, A.R. Compact diode-pumped 1.1 kW YbYAG Innoslab femtosecond amplifier. *Opt. Lett.* **2010**, *35*, 4169. [[CrossRef](#)]
19. Nubbemeyer, T.; Kaumanns, M.; Ueffing, M.; Gorjan, M.; Alismail, A.; Fattahi, H.; Brons, J.; Pronin, O.; Barros, H.G.; Major, Z.; et al. 1 kW, 200 mJ picosecond thin-disk laser system. *Opt. Lett.* **2017**, *42*, 1381. [[CrossRef](#)]
20. Eidam, T.; Hanf, S.; Seise, E.; Andersen, T.V.; Gabler, T.; Wirth, C.; Schreiber, T.; Limpert, J.; Tünnermann, A. Femtosecond fiber CPA system emitting 830 W average output power. *Opt. Lett.* **2010**, *35*, 94. [[CrossRef](#)]
21. Voronin, A.A.; Zheltikov, A.M.; Ditmire, T.; Rus, B.; Korn, G. Subexawatt few-cycle lightwave generation via multipetawatt pulse compression. *Opt. Commun.* **2013**, *291*, 299. [[CrossRef](#)]

22. Lassonde, P.; Mironov, S.; Fourmaux, S.; Payeur, S.; Khazanov, E.; Sergeev, A.; Kieffer, J.-C.; Mourou, G. High energy femtosecond pulse compression. *Laser Phys. Lett.* **2016**, *13*, 075401. [[CrossRef](#)]
23. Schulte, J.; Sartorius, T.; Weitenberg, J.; Vernaleken, A.; Russbueltdt, P. Nonlinear pulse compression in a multi-pass cell. *Opt. Lett.* **2016**, *41*, 4511. [[CrossRef](#)] [[PubMed](#)]
24. Ueffing, M.; Reiger, S.; Kaumanns, M.; Pervak, V.; Trubetskov, M.; Nubbemeyer, T.; Krausz, F. Nonlinear pulse compression in a gas-filled multipass cell. *Opt. Lett.* **2018**, *43*, 2070. [[CrossRef](#)] [[PubMed](#)]
25. Lavenu, L.; Natile, M.; Guichard, F.; Zaouter, Y.; Delen, X.; Hanna, M.; Mottay, E.; Georges, P. Nonlinear pulse compression based on a gas-filled multipass cell. *Opt. Lett.* **2018**, *43*, 2252. [[CrossRef](#)]
26. Kaumanns, M.; Pervak, V.; Kormin, D.; Leshchenko, V.; Kessel, A.; Ueffing, M.; Chen, Y.; Nubbemeyer, T. Multipass spectral broadening of 18 mJ pulses compressible from 1.3 ps to 41 fs. *Opt. Lett.* **2018**, *43*, 5877. [[CrossRef](#)]
27. Balla, P.; Bin Wahid, A.; Sytceovich, I.; Guo, C.; Viotti, A.-L.; Silletti, L.; Cartella, A.; Alisaukas, S.; Tavakol, H.; Grosse-Wortmann, U.; et al. Postcompression of picosecond pulses into the few-cycle regime. *Opt. Lett.* **2020**, *45*, 2572. [[CrossRef](#)]
28. Kaumanns, M.; Kormin, D.; Nubbemeyer, T.; Pervak, V.; Karsch, S. Spectral broadening of 112 mJ, 1.3 ps pulses at 5 kHz in a LG10 multipass cell with compressibility to 37 fs. *Opt. Lett.* **2021**, *46*, 929. [[CrossRef](#)]
29. Pfaff, Y.; Forster, C.; Barbiero, G.; Rampp, M.; Klingebiel, S.; Brons, J.; Teisset, C.Y.; Wang, H.; Jung, R.; Jaksic, J.; et al. Nonlinear pulse compression of a thin-disk amplifier and contrast enhancement via nonlinear ellipse rotation. *Opt. Express* **2022**, *30*, 10981. [[CrossRef](#)]
30. Weitenberg, J.; Vernaleken, A.; Schulte, J.; Ozawa, A.; Sartorius, T.; Pervak, V.; Hoffmann, H.-D.; Udem, T.; Russbueltdt, P.; Hänsch, T.W. Multi-pass-cell-based nonlinear pulse compression to 115 fs at 7.5 uJ pulse energy and 300 W average power. *Opt. Express* **2017**, *25*, 20502–20510. [[CrossRef](#)]
31. Fan, G.; Carpeggiani, P.A.; Tao, Z.; Coccia, G.; Safaei, R.; Kaksis, E.; Pugzlys, A.; Légaré, F.; Schmidt, B.E.; Baltuška, A. 70 mJ nonlinear compression and scaling route for an Yb amplifier using large-core hollow fibers. *Opt. Lett.* **2021**, *46*, 896–899. [[CrossRef](#)] [[PubMed](#)]
32. Nagy, T.; Hädrich, S.; Simon, P.; Blumenstein, A.; Walther, N.; Klas, R.; Buldt, J.; Stark, H.; Breitkopf, S.; Jójárt, P.; et al. Generation of three-cycle multi-millijoule laser pulses at 318 W average power. *Optica* **2019**, *6*, 1423. [[CrossRef](#)]
33. Mironov, S.Y.; Wheeler, J.; Gonin, R.; Cojocar, G.; Ungureanu, R.; Banici, R.; Serbanescu, M.; Dabu, R.; Mourou, G.; A Khazanov, E. 100 J-level pulse compression for peak power enhancement. *Quantum Electron.* **2017**, *47*, 173. [[CrossRef](#)]
34. Khazanov, E.A.; Mironov, S.Y.; Mourou, G. Nonlinear compression of high-power laser pulses: Compression after compressor approach. *Phys. Uspekhi* **2019**, *62*, 1096–1124. [[CrossRef](#)]
35. Bleotu, P.G.; Wheeler, J.; Mironov, S.Y.; Ginzburg, V.; Masruri, M.; Naziru, A.; Secareanu, R.; Ursescu, D.; Perez, F.; De Sousa, J.; et al. Post-compression of high-energy, sub-picosecond laser pulses. *High Power Laser Sci. Eng.* **2023**, *11*, e30. [[CrossRef](#)]

Disclaimer/Publisher's Note: The statements, opinions and data contained in all publications are solely those of the individual author(s) and contributor(s) and not of MDPI and/or the editor(s). MDPI and/or the editor(s) disclaim responsibility for any injury to people or property resulting from any ideas, methods, instructions or products referred to in the content.